ORIGINAL ARTICLE

Advanced Diffusion Models in Head and Neck Squamous Cell Carcinoma Patients: Goodness of Fit, Relationships among Diffusion Parameters and Comparison with Dynamic Contrast-Enhanced Perfusion

Noriyuki Fujima, MD, PhD[1]; Tomohiro Sakashita, MD, PhD[2]; Akihiro Homma, MD, PhD[2]; Yukie Shimizu, MD[1]; Atsushi Yoshida, MD, PhD[1]; Taisuke Harada, MD, PhD[1]; Khin Khin Tha, MD, PhD[3,4]; Kohsuke Kudo, MD, PhD[1] and Hiroki Shirato, MD, PhD[3,4]

[1] Department of Diagnostic and Interventional Radiology, Hokkaido University Hospital, Sapporo, Japan

[2] Department of Otolaryngology-Head and Neck Surgery, Hokkaido University Graduate School of Medicine, Sapporo, Japan

[3] Department of Radiation Medicine, Hokkaido University Graduate School of Medicine, Sapporo, Japan

[4] The Global Station for Quantum Medical Science and Engineering, Global Institution for collaborative research and education, Sapporo, Japan

Corresponding Author

Noriyuki Fujima

Department of Radiology, Hokkaido University Hospital

N15, W7, Kita-Ku, Sapporo 060-8638, Japan

Phone: +81-11-706-5977, Fax: +81-11-706-7876

E-mail: Noriyuki.Fujima@mb9.seikyou.ne.jp

Grant Support

The first author (Noriyuki Fujima) has received the grant support from Ministry of Education, Culture, Sports, Science and Technology – Japan (ID; 15K19761).

ABSTRACT

Purpose: We assessed advanced fitting models of diffusion weighted imaging (DWI) in head/neck squamous cell carcinoma (HNSCC) patients to determine the best goodness of fit and correlations among diffusion parameters. We compared these results with those of dynamic contrast-enhanced (DCE) perfusion parameters.

Materials and Methods: We retrospectively evaluated 32 HNSCC patients (12 sinonasal, 20 pharynx/oral cavity). The DWI acquisition used single-shot spin-echo echo-planar imaging (EPI) with 12 b-values (0–2000). We calculated 14 DWI parameters using mono-exponential, bi-exponential, and tri-exponential models, stretched exponential model (SEM) and diffusion kurtosis imaging (DKI) models. We compared each model's goodness of fit using the residual sum of squares (RSS), Akaike Information Criterion (AIC) and Bayesian information criterion (BIC) value. We determined the correlation between each pair of DWI parameters and between each DWI parameter and DCE perfusion parameter.

Results: The tri-exponential fit's RSS, AIC and BIC values were significantly smaller than those for bi-exponential fit. The RSS, AIC and BIC values of the SEM fit and DKI fit were significantly smaller than mono-exponential model. Significant correlations were observed in 30 pairs (sinonasal cavity) and 31 (sinonasal cavity group) among 91 DWI parameter combinations. Significant correlations were also observed in nine pairs (both sinonasal cavity and pharynx/oral cavity group) among 64 DWI/DCE perfusion parameter pairs, in particular, high positive correlations between the tri-exponential model's intermediate diffusion fraction (f_2) and the volume of the extracellular extravascular space per unit volume of tissue (v_e) were observed in both patient groups.

Conclusion: We identified several correlations between DWI parameters by advanced fitting models and correlations between DWI and DCE parameters. These will help determine HNSCC patients' detailed tissue structures.

Keywords: diffusion weighted imaging, advanced fitting models, head and neck squamous cell carcinoma, dynamic contrast-enhanced perfusion

Introduction

Diffusion-weighted imaging (DWI) is a well-known noninvasive technique that is used to obtain tissue microstructural information by measuring water diffusivity in various tissues, including cancer [1]. DWI signal intensity changes in different b-values were proposed to be caused by microstructural conditions such as cell density, length of cell membrane, cell size or shape, and the ratio of intracellular to extracellular space that influences the water diffusion [2, 3].

The apparent diffusion coefficient (ADC), calculated using the mono-exponential decay function of DWI signal intensity with two or more b-values, has been reported to be useful in head and neck squamous cell carcinoma (HNSCC) cases for differentiating benign and malignant tissues, and to assess therapeutic efficacy and predict treatment outcomes [4, 5]. Although the biological characteristics of sinonasal and pharynx SCC are somewhat different and these two types of HNSCC also slightly differ in regard to characteristics such as causes, risk factors, frequency of lymph node and distant metastases, and treatment strategies, the utility of the ADC was reported for both types of HNSCC [4–6]. However, the water diffusion behavior in cancer tissues is complicated, and it is difficult to explain the water diffusion behavior in a completely free water diffusion model using the mono-exponential decay function. This is due to the complex structures such as the capillary network and cell membranes in each pixel. Such a complicated structure can cause the behavior of water diffusion to resemble non-Gaussian (restricted) diffusion rather than Gaussian diffusion calculated by mono-exponential fitting.

Advanced fitting models for DWI were recently described [7-13]. For example, a

model using intravoxel incoherent motion (IVIM) was proposed; by using the bi-exponential decay function, it divides the fast and slow diffusion components, which reflects the true tissue diffusivity and capillary perfusion, respectively [7, 8]. A tri-exponential fitting model was also described that divides the three different diffusion components by using a tri-exponential decay function [9, 10]. This multi-component analysis by a tri-exponential model may reveal more details of the water diffusion in cancer tissue compared to a bi-exponential model. A stretched exponential model (SEM) diffusion model was described as follows: the SEM model was used to describe the heterogeneity of water diffusion in each voxel. In this model, to obtain a good fit to multiple b-value signal decay data, the two parameters of diffusion heterogeneity and diffusion coefficient are respectively calculated [11, 12]. A diffusion kurtosis imaging (DKI) model also uses the diffusion distribution information. In this method, the degree of difference (= kurtosis value) from the Gaussian distribution in the water diffusion distribution is calculated by the Taylor expansion, and this kurtosis value was used for the correction of the multiple b-value signal decay curve [8, 13]. These different non-Gaussian diffusion models can fit the diffusion signal decay curve more precisely, reflecting tissue characteristics such as lesions of the capillary network, the extracellular extravascular space (EES), and the cellular space more clearly and in greater detail.

The three purposes of the present study were to: (1) determine which diffusion model best fitted the multiple b-value signal decay curve, (2) assess the correlations among the multiple diffusion parameters obtained by the various fitting models, and (3) identify the correlations between the diffusion parameter derived from the multiple fitting models and

the parameters derived using the dynamic contrast-enhanced (DCE) perfusion technique.

Materials and Methods

Patients

The protocol of this retrospective study was approved by our institutional review board, and written informed consent was waived. We evaluated the cases of 32 patients with HNSCC who were treated at our hospital during the roughly 3-year period from September 2012 to November 2015. All patients fulfilled the following inclusion criteria: (1) the patient was first diagnosed (not a recurrent case) histopathologically as having HNSCC, (2) magnetic resonance imaging (MRI) including both multi b-point diffusion and DCE perfusion MRI were performed within one scanning before any treatment. The primary lesions of 12 patients were in the sinonasal cavity (10 males and two females; mean age 63.6 yrs, range 47–77 yrs; T stage of T3 in two patients, T4a in seven patients, and T4b in three patients). The primary lesions of the other 20 patients were in the pharynx or oral cavity (17 males and three females; mean age 61.2 yrs, range 45–77 yrs; T2 stage in four patients, T3 in four patients, T4a in seven, and T4b in five). The lesion location in the patients with a pharynx SCC included the oropharynx and hypopharynx only; there was no nasopharynx SCC.

Imaging protocol

DWI acquisition

All MR imaging was performed using a 3.0 Tesla unit (Achieva TX; Philips

Healthcare, Best, Netherlands) with a 16-channel neurovascular coil. The DWI acquisition used single-shot spin-echo echo-planar imaging (EPI) with three orthogonal motion probing gradients. Twelve b-values (0, 10, 20, 30, 50, 80, 100, 200, 400, 800, 1000, and 2000 s/mm^2) were used. Diffusion images were acquired with a three-directional trace scheme for each b-value. The other imaging parameters were: TR, 4500 ms; TE, 64 ms; DELTA (large delta; gradient time interval), 30.1 ms; delta (small delta; gradient duration), 24.3 ms; flip angle, 90°; field of view (FOV), 230×230 mm; 64×64 matrix; slice thickness, 5 mm×20 slices; voxel size 3.59×3.59×5.00 mm; parallel imaging acceleration factor, 2; the number of signal averages = b-value of 0–100 s/mm^2 (one average), 200–800 s/mm^2 (two averages) and 1000–2000 s/mm^2 (three averages); scanning time, 4 min 37 s.

DCE perfusion acquisition

The DCE perfusion data were acquired after a bolus injection of 0.2 mmol gadolinium/kg (gadopentetate dimeglumine, Magnevist, Bayer Schering Pharma, Berlin, Germany; or gadodiamide, Omniscan, GE Healthcare, Milwaukee, WI, USA) at 2 mL/s using a power injector, followed by 15 mL of saline flush. Image acquisition was performed using a three-dimensional (3D)-T1 fast field echo (T1-FFE) sequence. The MR parameters for the dynamic data acquisition were as follows: TR, 6.1 ms; TE, 1.5 ms; flip angle, 15°; keyhole imaging percentage, 50 %; parallel imaging acceleration (SENSE) factor, 2.3; scan percentage, 0.6; temporal resolution, 3.2 s; dynamic phase, 64 phases; acquired matrix, 256 × 128 (reconstructed matrix, 256 × 256) in 230 × 230 mm, FOV (pixel size, 0.94 × 0.93 mm); slice thickness, 3 mm × 31 slices; scanning time, 3 min 51 s.

Data analysis

Diffusion data calculation

From the diffusion signal data, we calculated each parameter of the mono-exponential function (apparent diffusion coefficient; ADC), the bi-exponential function (perfusion fraction f, the pseudo-diffusion coefficient D*, and the true diffusion coefficient D), the tri-exponential function (perfusion-related diffusion fraction f_1 and coefficient D_1, intermediate diffusion fraction f_2 and coefficient D_2, slow diffusion fraction f_3 and coefficient D_3), the DKI (kurtosis value K and the kurtosis-corrected diffusion coefficient D_k), and the SEM (diffusion heterogeneity α and the distributed diffusion coefficient DDC). Using the signal intensity of all 12 b-values, we calculated the bi-exponential and tri-exponential function parameters. The assessment of the ADC and the DKI and SEM usually targeted the tissue diffusion other than the perfusion-related diffusion, because these models are usually used to analyze the tissue diffusion coefficient and tissue heterogeneity without including the perfusion-related signal — unlike bi-exponential and tri-exponential models, which target the DW-signal including the perfusion-related signal intensity. We used the signal intensity of six b-values (0, 200, 400, 800, 1000 and 2000 s/mm^2) for the parameter calculation of ADC, DKI and SEM. To perform these parameter calculations, we used the following equations [7, 9-13]:

$$\frac{S_{(b)}}{S_0} = e^{-b \cdot ADC} \tag{1}$$

$$\frac{S_{(b)}}{S_0} = f \cdot e^{-b \cdot D^*} + (1 - f) \cdot e^{-b \cdot D} \tag{2}$$

$$\frac{S_{(b)}}{S_0} = f_1 \cdot e^{-b \cdot D_1} + f_2 \cdot e^{-b \cdot D_2} + f_3 \cdot e^{-b \cdot D_3} \tag{3}$$

$$\frac{S_{(b)}}{S_0} = \exp\left[- b * D_k + \frac{1}{6} * b^2 * D_k{}^2 * K \right] \tag{4}$$

$$\frac{S_{(b)}}{S_0} = e^{-(b \cdot DDC)^{\alpha}} \tag{5}$$

where $S_{(b)}$ is the signal intensity at the b-value denoted by the subscript, S_0 is the signal intensity at the b-value of 0, and *b* is b-factor in Eqs. (1) to (5). In tri-exponential fitting of Eq (3), the sum of the three parameters f_1 ,f_2 and f_3 became 1. We fitted the signal intensity of b-values in Eqs. (1) to (5) with least square fitting using the Levenberg-Marquardt algorithm. To improve the fitting accuracy and to prevent overfitting in all b-value fitting analyses of the bi-exponential and tri-exponential models, we performed the fitting procedure by the following methods. In the bi-exponential analysis, first, the data of b >200 s/mm^2 were fitted for the single parameter D by the mono-exponential function. In the second step, the curve was fitted for f and D* over all b-values by using Eq. (2), while keeping D constant. The details of this method are provided in a previous report [7]. In the tri-exponential analysis, three-step fitting was performed as follows. We first performed mono-exponential fitting with large b-values (800, 1000 and 2000 s/mm^2) to obtain D_3,

followed by bi-exponential fitting with b-values of ≥ 200 s/mm^2 to obtain D_2. We next performed tri-exponential fitting by using Eq. (3) with all b-values to obtain D_1, f_1, f_2 and f_3. The details of this method are also described in a previous report [10]. All parameter calculations were performed on a pixel-by-pixel basis, and finally, all DW model parameter maps were respectively obtained on a pixel-by-pixel basis.

DCE perfusion data calculation

Using the DCE dynamic dataset, we calculated the DCE perfusion parameters K^{trans} (the volume transfer constant between the blood plasma and the EES), v_p (the plasma volume fraction) v_e (the volume of EES per unit volume of tissue), K_{ep} (the ratio of K^{trans} to v_e) according to the method described based on the two-compartment model; the details of this model are described elsewhere [14]. All DCE parameters were obtained on a pixel-by-pixel basis, and all DCE parameter maps were also obtained on a pixel-by-pixel basis. We used MATLAB ver. 2012a software (MathWorks, Natick, MA) for the calculations of the DWI and DCE perfusion parameters.

ROI setting

A polygonal region of interest (ROI) was placed to delineate the whole tumor lesion in the slice, carefully avoiding necrotic areas, cystic formations and large vessels. First, the ROI was placed on the last phase of the DCE images. This ROI was then placed on the diffusion b0 image with manual adjustment by using anatomical information for the fixation of its location. Finally, all diffusion parameter maps in this ROI were used for the

analysis (Fig. 1). ROI placements were performed by a single neuroradiologist with 19 years of experience. All pixels in the tumor ROI were determined as the target of analysis.

Assessment of the goodness of fit

For the assessment of goodness of fit provided by each model, we calculated the residual sum of square (RSS) on an ROI basis, which is the sum of the differences between observed and expected outcome values. We also calculated the Akaike information criterion (AIC) and the Bayesian information criterion (BIC) on an ROI basis. The AIC and BIC are statistical information criteria used to determine which model fits best to sample observations, reported as follows [10, 15]:

$$AIC=N*\ln(SS)+2q \quad (6)$$

$$BIC=N*\ln(SS/N)+q*\ln(N) \quad (7)$$

where N is the number of data points, SS is the sum of squared errors, and q is the number of estimated parameters, as described [10, 15]. In tri-exponential fitting, because the sum of the three parameters f_1 ,f_2 and f_3 became 1, the tri-exponential model parameter was considered to have five independent parameters (not six parameters) in the AIC and BIC calculation process. Finally, the AIC and BIC value in each pixel in the tumor ROI was calculated.

Statistical analysis

For the assessment of goodness of fit, we compared the RSS values between the diffusion fitting models with the use of all b-values (bi-exponential and tri-exponential

fitting), using the paired t-test. We also compared the RSS values between the diffusion fitting models with the b-value of tissue diffusion (mono-exponential, DKI and SEM) by performing a multiple comparison (analysis of variance [ANOVA], post hoc; Tukey's method). The AIC values between all fitting models were also compared by a multiple comparison (ANOVA, post hoc; Tukey's method).

For all of the parameters obtained by the diffusion fitting models, we compared the variables using Pearson's correlation coefficient for the assessment of the relationships between these variables. We set the following correlation coefficient categories: $r<0.2$, very weak correlation; $r=0.2–0.4$, weak correlation; $r=0.41–0.6$, fair correlation; $r=0.61–0.8$, moderate correlation; $r\geq0.81$, good correlation. We also used Pearson's correlation coefficient to determine the correlations of all pairs of diffusion and DCE perfusion parameters. Because the biological characteristics are somewhat different between sinonasal cavity SCCs and pharynx/oral cavity SCCs [16], we performed the correlation analysis between DWI parameters and also the correlation analysis between DWI and DCE perfusion parameters by dividing the total patient series into the sinonasal cavity group and the pharynx/oral cavity group. All correlation analyses between diffusion parameters and between diffusion and DCE perfusion parameters were performed based on the pixel-by-pixel correlation. Because the in-plane matrix was different between the diffusion parameter map and the DCE perfusion parameter map, we used the mean value of 4×4 pixels (total 16 pixels) on the DCE perfusion parameter map for the correlation analysis so that it corresponded to one pixel on the diffusion parameter map, based on acquired scan matrix that in-plane matrix of DCE images (256×256) were respectively 4 times larger in

both the x (anterior-posterior) and y (right-left) axes compared to the matrix of DW images (64×64).

In addition, we compared all of the parameters obtained by the multi-diffusion models and DCE perfusion between the sinonasal cavity group and the pharynx/oral cavity group, using the unpaired t-test. The mean value in the tumor ROI in each parameter map was used to determine its tumor's parameter value. A p-value of 0.05 was accepted as significant.

Results

We analyzed a total of 1,095 pixels on diffusion parameter maps from 12 tumor ROIs of the sinonasal SCCs and a total of 1,421 pixels on diffusion parameter maps from 20 tumor ROIs of the pharynx/oral cavity SCCs. We were able to successfully perform the parameter calculations in each diffusion fitting model. Each diffusion model fitting curve and DW-signal decay plot shown in representative pixels are presented in Figures 2 and 3. The details of the calculated parameter are summarized in Table 1.

In our assessment of goodness of fit, the RSS, AIC and BIC value of the tri-exponential fit was significantly smaller than that of the bi-exponential fit ($p<0.01$, respectively). The RSS, AIC and BIC values of the SEM fit and the DKI fit were both smaller than that of the mono-exponential model ($p<0.001$, respectively). There was no significant difference between the RSS, AIC and BIC values of the SEM and DKI models. The RSS, AIC and BIC values are summarized in Table 2.

The assessment of the correlations between all pairs of calculated DWI parameters

revealed significant correlations in 30 pairs among the total of 91 pairs of parameter combinations in the sinonasal cavity group, and in 31 pairs in the pharynx/oral cavity group. The correlation coefficients are summarized in Table 3.

In our assessment of the correlations of DCE perfusion parameters and each fitting model diffusion parameters, we observed significant correlations in nine pairs among the total of 64 pairs of parameter combinations in both of the sinonasal cavity and the pharynx/oral cavity group. Of particular note, a moderate positive correlation coefficient between the f_2 values from the tri-exponential model and v_e was observed in both the sinonasal and pharynx/oral cavity groups. All of the correlation coefficients between the perfusion and diffusion parameters are summarized in Table 4.

In our comparison of all parameters obtained by the multi DW-models and DCE perfusion between the sinonasal cavity group and the pharynx/oral cavity group, only v_p was significantly different ($p<0.01$).

Discussion

All of the DWI parameters obtained by the various diffusion models were successfully calculated in this study, and the results indicated that a better fit was obtained by using the tri-exponential model compared to the bi-exponential model in all b-value datasets. In addition, the SEM and the DKI model were better than the mono-exponential model in the high b-value range (i.e., 200–2000). To the best of our knowledge, only a few studies have investigated relationships among imaging parameters derived from advanced diffusion models and DCE-MRI in HNSCC [17–19], and the present study is the first to

report results obtained by the stretched exponential and tri-exponential models for the assessment of HNSCC.

Related to the diffusion parameters in the analysis of all b-values, past reports stated that tri-exponential fitting enabled a division of the perfusion-related signal, the intermediate diffusion signal and slow restricted diffusion [10]. The microstructural content of cancer tissue is conventionally divided into the perfusion-related lesion, extravascular extracellular space and cellular compartment [20]. Our present findings indicated a certain degree of correlation between v_e in DCE perfusion and f_2 in the tri-exponential model. The diffusion value D_2 in the f_2 compartment was approx. 1.0–1.5 in most of the lesions in all of the delineated ROIs. We speculate that the second diffusion component f_2 mainly reflects the water diffusion in the EES, and we suspect that a water diffusion coefficient of approx. 1.0–1.5 might reflect the water diffusivity of the EES, although there will be some overlap with other compartments of water diffusion such as part of the very-slow-flow microcirculation or a cellular compartment with large water permeability of the cell membrane. In addition, the tri-exponential parameter f_1 was correlated with the plasma volume v_p; this indicated that f1 reflected mainly the perfusion-related space. In contrast, D_3 was not correlated with any parameter of DCE perfusion. However, considering that the tissue compartment of HNSCC has been described as mainly the perfusion fraction, EES and cellular compartment, we also speculated that D_3 might reflect mainly the cellular compartment, and it may also reflect a narrow EES with a high cellular density area. In contrast, a number of correlations were observed between other pairs of diffusion coefficients, i.e., ADC, D, D_2, D_3, DDC and D_k. The microstructural information such as

the EES or cellular space reflected by these diffusion coefficients was probably overlapped to a degree. Bi-exponential fitting can divide the fast and slow water diffusion, but in the present study we observed that this fitting method was not superior to the tri-exponential fitting in regard to the goodness of fitting in the multiple (i.e., 12) b-value data used in the current study. This is probably because the slow water diffusion component included the two micro-components of the EES and cellular compartment, and the water diffusion in these two compartments will be quite different because of the difference in the microstructural membrane. Bi-exponential fitting may not be sufficient to handle two such slow compartments, because this model provides only one parameter for the calculation of the slow diffusion component; the slow diffusion coefficient obtained by bi-exponential model will contain both the EES and the cellular component, and thus the fitting level will not be sufficient.

Regarding the diffusion parameters with a high b-value that target the tissue water diffusion, in the heterogeneity of water diffusion distribution, the fitting level of α obtained by using the SEM model did not provide very different RSS, AIC and BIC values compared to the kurtosis value obtained by DKI model, and thus a significant difference was not observed. In contrast, the α and kurtosis values were well inversely correlated. Both of these parameters assess the degree of the difference from the normal distribution, which means that both parameters reflected the diffusion heterogeneity of the water diffusion distribution, although the kurtosis model used the approximation of the signal decay curve in multiple b-value data using a quadratic equation, whereas the SEM used the exponential function. In addition, in our comparison of the DKI model and the SEM, the

DDC and D_k values both ranged within almost the same values (approx. 1.0–1.5), and a positive correlation was also detected. These values were moderately or well correlated with the tri-exponential D_2 value. Based on these results, we speculate the D_2, DDC and D_k all reflect, to some extent, the intermediate water diffusion which may arise mainly due to the water diffusion from the EES, if these parameters are calculated using the dataset of 12 b-values as done in the present study. We suspect that the K value and α can be influenced by the balance of the diffusion degree or compartment ratio between the EES and other components such as the cellular component which might be affected by the cell shape, cell size, cell density and cell membrane permeability [21, 22].

Our study has several limitations. First, only a fixed number (n=12) of b-value data was used. The component detected by the various diffusion models will vary depending on the arrangement/range of b-values. If a very low b-value dataset such as one with five intervals from b=0 to 50 is acquired, the perfusion-related diffusion can be divided into very fast (like an arterial component) and slow perfusion or a venous flow component. A very fast diffusion component was recently reported in a liver study that used a tri-exponential function [23]. In addition, increasing data points in large b-values can influence the tissue diffusion coefficient, the kurtosis value obtained by DKI, and the α value obtained by the SEM. However, considering the acquisition time and signal-to-noise ratio level, we felt that a very detailed analysis would not be appropriate for daily clinical use. Second, we did not perform a repeatability analysis. The repeatability of a perfusion-related diffusion coefficient obtained with bi-exponential fitting was reported to be insufficient [24]. It was still unclear whether sufficient repeatability was obtained or not

for perfusion-related diffusion parameters when these advanced fitting models are used as fitting methods. Third, our discussion of the present findings is based on the correlation of DCE perfusion parameters, and we did not compare the results to the histological specimens. Further analysis will be required in the future. Fourth, the results of this study revealed a significant difference in v_p between sinonasal and pharynx SCCs; this finding might indicate a biological difference related to the two different primary lesions. However, the diffusion parameters showed no significant differences between these two types of HNSCC. Further sub-group analyses with detailed divisions such as T-stage, genomic information such as the human papillomavirus status, and histological differentiation are necessary to confirm the presence of differences between sinonasal and pharynx SCCs.

In conclusion, the tri-exponential fitting method may divide the slow diffusion component into two elements such as the EES and the cellular component's dominant space. In addition, the kurtosis value and α provided by the stretched exponential model had a negative correlation; it is possible that these two parameters reflect something similar or represent behavior related to the tissue heterogeneity. These fitting methods of water diffusion behavior can be useful for investigations of the detailed tissue structure for patients with HNSCC.

References

[1] Iima M, Le Bihan D. Clinical Intravoxel incoherent motion and diffusion MR imaging: past, present, and future. Radiology 2016;278:13–32. doi: 10.1148/radiol.2015150244.

[2] Le Bihan D. Apparent diffusion coefficient and beyond: what diffusion MR imaging can tell us about tissue structure. Radiology 2013;268:318–22. doi: 10.1148/radiol.13130420.

[3] Eida S, Van Cauteren M, Hotokezaka Y, Katayama I, Sasaki M, Obara M, Okuaki T, Sumi M, Nakamura T. Length of intact plasma membrane determines the diffusion properties of cellular water. Sci Rep 2016;6:19051. doi:10.1038/srep19051.

[4] Jansen JF, Parra C, Lu Y, Shukla-Dave A. Evaluation of head and neck tumors with functional MR imaging. Magn Reson Imaging Clin N Am 2016;24:123–33. doi: 10.1016/j.mric.2015.08.011.

[5] Srinivasan A, Mohan S, Mukherji SK. Biologic imaging of head and neck cancer: the present and the future. AJNR Am J Neuroradiol 2012;33:586–94. doi: 10.3174/ajnr.A2535.

[6] Fujima N, Yoshida D, Sakashita T, Homma A, Tsukahara A, Shimizu Y, Tha KK, Kudo K, Shirato H. Prediction of the treatment outcome using intravoxel incoherent motion and diffusional kurtosis imaging in nasal or sinonasal squamous cell carcinoma patients. Eur Radiol 2016; Jun 2. [Epub ahead of print].

[7] Fujima N, Yoshida D, Sakashita T, Homma A, Tsukahara A, Tha KK, Kudo K,

Shirato H. Intravoxel incoherent motion diffusion-weighted imaging in head and neck squamous cell carcinoma: assessment of perfusion-related parameters compared to dynamic contrast-enhanced MRI. Magn Reson Imaging 2014;32:1206–13. doi: 10.1016/j.mri.2014.08.009.

[8] Fujima N, Kudo K, Yoshida D, Homma A, Sakashita T, Tsukahara A, Khin Khin T, Yuri Z, Satoshi T, Hiroki S. Arterial spin labeling to determine tumor viability in head and neck cancer before and after treatment. J Magn Reson Imaging 2014;40(4):920–8. doi: 10.1002/jmri.24421.

[9] Ohno N, Miyati T, Kobayashi S, Gabata T. Modified triexponential analysis of intravoxel incoherent motion for brain perfusion and diffusion. J Magn Reson Imaging 2016;43:818–23. doi: 10.1002/jmri.25048.

[10] Ueda Y, Takahashi S, Ohno N, Kyotani K, Kawamitu H, Miyati T, Aoyama N, Ueno Y, Kitajima K, Kawakami F et al. Triexponential function analysis of diffusion-weighted MRI for diagnosing prostate cancer. J Magn Reson Imaging 2016;43:138–48. doi: 10.1002/jmri.24974.

[11] Yuan J, Yeung DK, Mok GS, Bhatia KS, Wang YX, Ahuja AT, King AD. Non-Gaussian analysis of diffusion weighted imaging in head and neck at 3T: a pilot study in patients with nasopharyngeal carcinoma. PloS One 2014;9:e87024. http://dx.doi.org/10.1371/journal.pone.0087024.

[12] Bai Y, Lin Y, Tian J, Shi D, Cheng J, Haacke EM, Hong X, Ma B, Zhou J, Wang M. Grading of gliomas by using monoexponential, biexponential, and stretched exponential diffusion-weighted MR imaging and diffusion kurtosis MR imaging.

Radiology 2016;278:496–504. doi: 10.1148/radiol.2015142173.

[13] Chen Y, Ren W, Zheng D, Zhong J, Liu X, Yue Q, Liu M, Xiao Y, Chen W, Chan Q et al. Diffusion kurtosis imaging predicts neoadjuvant chemotherapy responses within 4 days in advanced nasopharyngeal carcinoma patients. J Magn Reson Imaging 2015;42:1354–61. doi: 10.1002/jmri.24910.

[14] Chikui T, Kitamoto E, Kawano S, Sugiura T, Obara M, Simonetti AW, Hatakenaka M, Matsuo Y, Koga S, Ohga M et al. Pharmacokinetic analysis based on dynamic contrast-enhanced MRI for evaluating tumor response to preoperative therapy for oral cancer. J Magn Reson Imaging 2012;36:589–97. doi: 10.1002/jmri.23704.

[15] Tijssen RH, Jenkinson M, Brooks JC, Jezzard P, Miller KL. Optimizing RetroICor and RetroKCor corrections for multi-shot 3D FMRI acquisitions. NeuroImage 2014;84:394–405. http://dx.doi.org/10.1016/j.neuroimage.2013.08.062.

[16] Fujima N, Yoshida D, Sakashita T, Homma A, Tsukahara A, Tha KK, Kudo K, Shirato H. Usefulness of pseudocontinuous arterial spin-labeling for the assessment of patients with head and neck squamous cell carcinoma by measuring tumor blood flow in the pretreatment and early treatment period. AJNR Am J Neuroradiol 2016;37:342–8. doi: 10.3174/ajnr.A4513.

[17] Han M, Kim SY, Lee SJ, Choi JW. The correlations between MRI perfusion, diffusion parameters, and 18F-FDG PET metabolic parameters in primary head-and-neck cancer: a cross-sectional analysis in single institute. Medicine 2015;94:e2141. doi: 10.1097/MD.0000000000002141.

[18] Jansen JF, Stambuk HE, Koutcher JA, Shukla-Dave A. Non-gaussian analysis of

diffusion-weighted MR imaging in head and neck squamous cell carcinoma: A feasibility study. AJNR Am J Neuroradiol 2010;31:741–748. doi: 10.3174/ajnr.A1919.

[19] Lu Y, Jansen JF, Mazaheri Y, Stambuk HE, Koutcher JA, Shukla-Dave A. Extension of the intravoxel incoherent motion model to non-gaussian diffusion in head and neck cancer. J Magn Reson Imaging 2012;36:1088–96. doi: 10.1002/jmri.23770

[20] Panagiotaki E, Walker-Samuel S, Siow B, Johnson SP, Rajkumar V, Pedley RB, Lythgoe MF, Alexander DC. Noninvasive quantification of solid tumor microstructure using VERDICT MRI. Cancer Res 2014;74:1902–12. doi: 10.1158/0008-5472.CAN-13-2511.

[21] Vorisek I, Hajek M, Tintera J, Nicolay K, Sykova E. Water ADC, extracellular space volume, and tortuosity in the rat cortex after traumatic injury. Magn Reson Med 2002;48:994–1003. doi: 10.1002/mrm.10305.

[22] Xu J, Xie J, Jourquin J, Colvin DC, Does MD, Quaranta V, Gore JC. Influence of cell cycle phase on apparent diffusion coefficient in synchronized cells detected using temporal diffusion spectroscopy. Magn Reson Med 2011;65):920–6. doi: 10.1002/mrm.22704.

[23] Cercueil JP, Petit JM, Nougaret S, Soyer P, Fohlen A, Pierredon-Foulongne MA, Schembri V, Delhom E, Schmidt S, Denys A et al. Intravoxel incoherent motion diffusion-weighted imaging in the liver: comparison of mono-, bi- and tri-exponential modelling at 3.0-T. Eur Radiol 2015;25):1541–50. doi: 10.1007/s00330-014-3554-6.

[24] Kakite S, Dyvorne H, Besa C, Cooper N, Facciuto M, Donnerhack C, Taouli B. Hepatocellular carcinoma: short-term reproducibility of apparent diffusion coefficient and intravoxel incoherent motion parameters at 3.0T. J Magn Reson Imaging 2015;41:149–56. doi: 10.1002/jmri.24538.

Table title and Figure legend

Table 1. DWI parameters of each model in all 32 patients with head/neck squamous cell carcinoma

	Sinonasal cavity	Oropharynx/oral cavity
ADC	1.04±0.25	0.99±0.29
D*	22.2±14.4	18.7±13.9
f	0.14±0.07	0.12±0.06
D	0.79±0.14	0.78±0.22
f_1	0.13±0.1	0.13±0.09
f_2	0.2±0.11	0.23±0.13
f_3	0.67±0.16	0.64±0.19
D_1	23.1±16.3	19.6±16.7
D_2	1.19±0.29	1.13±0.28
D_3	0.63±0.16	0.59±0.18
α	0.65±0.14	0.66±0.17
DDC	1.17±0.28	1.19±0.36
D_k	1.31±0.25	1.29±0.33
K	0.81±0.13	0.84±0.19
K^{trans}	26.5±6.8	27.6±5.9
V_p	7.39±2.9	4.48±1.5
V_e	23.5±7.2	19.7±6.4
K_{ep}	1.25±0.62	1.46±0.5

Table 1 footnote: Data are mean ± SD. ADC: apparent diffusion coefficient ($\times10^{-3}$ mm^2/s), D: true diffusion coefficient ($\times10^{-3}$ mm^2/s), f: perfusion fraction ($\times10^2$ %), D*: fast diffusion coefficient ($\times10^{-3}$ mm^2/s), f_1: perfusion-related diffusion fraction ($\times10^2$ %), f_2: intermediate diffusion fraction ($\times10^2$ %), f_3: slow diffusion fraction ($\times10^2$ %), D_1:

perfusion-related diffusion coefficient ($\times 10^{-3}$ mm^2/s), D_2: intermediate diffusion coefficient ($\times 10^{-3}$ mm^2/s), D_3: slow diffusion coefficient ($\times 10^{-3}$ mm^2/s), α: diffusion heterogeneity (dimensionless), DDC: distributed diffusion coefficient ($\times 10^{-3}$ mm^2/s), K: kurtosis value (dimensionless), D_k: kurtosis corrected diffusion coefficient ($\times 10^{-3}$ mm^2/s), K^{trans}: volume transfer constant between blood plasma and EES (min^{-1}), v_p: plasma volume fraction (dimensionless) v_e: the volume of EES per unit volume of tissue (dimensionless), K_{ep}: the ratio of the K^{trans} to v_e (min^{-1}).

Table 2. The RSS and AIC values for the Sinonasal Cavity cases (n=12) and Pharynx/Oral Cavity cases (n=20).

	Sinonasal Cavity			
	No. of b-points	RSS	AIC	BIC
Bi-exponential	12	6186±2727	109±7.5	82.3±6.7
Tri-exponential	12	2739±1448	104.4±6.8	77.8±6.1
Mono-exponential	6	5218±2987	61.7±5.6	44.1±4.6
Stretched-exponential	6	1541±997	52.9±6.1	36.8±4.3
Diffusion kurtosis	6	1516±971	53.3±4.8	36.7±4.2

	Pharynx/Oral Cavity			
	No. of b-points	RSS	AIC	BIC
Bi-exponential	12	7977±2854	113.2±8.9	85.4±7.2
Tri-exponential	12	4686±2568	109.2±7.8	82.4±5.8
Mono-exponential	6	7065±3678	63.3±5.9	46.7±4.8
Stretched-exponential	6	3630±1678	58.7±5.4	40±4.1
Diffusion kurtosis	6	3675±1529	59.4±5.5	40.8±4.5

Table 2 footnote: Data are mean ± SD. AIC: Akaike Information Criterion, BIC: Bayesian information criterion, RSS: the residual sum of squares.

Table 3. The correlation coefficient of each pair among all diffusion parameters

Sinonasal cavity

	ADC	D*	f	D	f_1	f_2	f_3	D_1	D_2	D_3	α	DDC	D_k	K
ADC		0.19	0.13	0.75*	0.34	0.5	0.08	-0.21	0.68*	0.45*	0.22	0.93*	0.88*	-0.42*
D*			0.25	-0.06	0.28	-0.31	0.01	0.48*	-0.28	0.09	-0.05	0.27	0.19	0.02
f				-0.19	0.72*	-0.39	-0.06	0.23	0.34	0.05	-0.27	0.23	0.37	0.17
D					0.13	0.27	0.29	-0.16	0.49*	0.81*	0.46*	0.71*	0.65*	-0.56*
f_1						-0.46	-0.08	0.11	0.21	0.35	-0.29	0.33	0.28	-0.14
f_2							-0.53*	-0.21	0.63*	-0.38	0.4	0.49*	0.57*	-0.19
f_3								0.05	-0.49*	0.15	-0.38	-0.34	-0.4	0.27
D_1									-0.39	-0.13	-0.14	0.08	0.07	0.23
D_2										0.32	0.26	0.68*	0.63*	-0.43*
D_3											0.46*	0.46*	0.43*	-0.59*
α												0.22	0.03	-0.7*
DDC													0.82*	-0.45*
D_k														-0.42*
K														

Pharynx/Oral cavity

	ADC	D*	f	D	f_1	f_2	f_3	D_1	D_2	D_3	α	DDC	D_k	K
ADC		0.33	0.27	0.65*	0.29	0.57*	0.18	0.17	0.68*	0.47*	0.26	0.92*	0.86*	-0.42*
D*			0.17	0.33	0.39	0.17	0.03	0.55*	0.12	0.07	0.1	0.29	-0.08	-0.03
f				0.27	0.7*	0.04	-0.33	0.09	0.45	0.24	-0.09	0.31	0.34	-0.22
D					0.16	0.18	0.31	0.37	0.61*	0.8*	0.48*	0.65*	0.62*	-0.62*
f_1						-0.31	-0.15	0.39	0.34	0.33	-0.29	0.32	0.33	-0.09
f_2							-0.5*	0.13	0.62*	-0.35	-0.11	0.59*	0.6*	-0.18
f_3								-0.03	-0.46*	0.2	-0.45	0.14	0.11	0.37
D_1									0.19	0.18	-0.03	0.18	0.23	-0.21
D_2										0.35	0.31	0.7*	0.68*	-0.42*
D_3											0.53*	0.47*	0.44*	-0.61*
α												0.34	0.33	-0.77*
DDC													0.85*	-0.43*

D_k		-0.42*
K		

Table 3 footnote: Data are Pearson's correlation coefficients. *p<0.05. Abbreviations are explained in the Table 1 footnote.

Table 4. The correlation coefficients between diffusion parameters and DCE perfusion parameters

	Sinonasal cavity			
	K^{trans}	V_p	Ve	Kep
ADC	0.22	0.21	0.45*	0.33
D*	0.38	0.31	0.06	0.16
f	0.51*	0.53*	-0.21	0.28
D	0.12	0.11	-0.18	-0.02
f_1	0.57*	0.57*	-0.27	0.45
f_2	-0.24	-0.5	0.65*	-0.3
f_3	-0.19	-0.12	-0.42	-0.31
D_1	0.39	0.04	0.02	0.14
D_2	0.29	0.15	0.58*	0.29
D_3	0.3	0.35	0.03	0.14
α	0.03	-0.31	0.13	-0.26
DDC	0.23	0.26	0.51*	0.36
D_k	0.29	0.26	0.52*	0.38
K	-0.11	-0.06	0.3	0.05
	Pharynx/Oral cavity			
	K^{trans}	V_p	Ve	Kep
ADC	0.19	0.13	0.43*	0.23

D*	0.36	-0.31	0.19	0.07
f	0.49*	0.55*	-0.06	0.33
D	-0.11	0.06	0.03	0.06
f_1	0.57*	0.59*	-0.31	0.48
f_2	-0.14	-0.45	0.64*	-0.39
f3	-0.21	0.02	-0.39	-0.25
D_1	0.39	-0.14	-0.05	0.05
D_2	0.06	-0.13	0.59*	0.31
D_3	0.21	0.07	-0.09	0.13
α	0.04	0.08	-0.1	-0.24
DDC	0.24	0.12	0.42*	0.24
D_k	0.15	0.11	0.43*	0.32
K	0.24	0.05	-0.03	0.09

Table 4 footnote: Data are Pearson's correlation coefficients. *p<0.05.

Fig. 1. ROI placement on the DWI and DCE perfusion images. A polygonal ROI was used for the delineation of the whole tumor. Necrotic areas, cystic formations and large vessels were carefully avoided. First, this ROI was placed on the last phase of DCE images (a). This ROI was then placed on the diffusion b0 image with manual adjustment based on anatomical information for the fixation of its location (b; large arrow). Finally, all diffusion parameter maps in this ROI were used for the analysis (b; small arrow).

Fig. 2. Bi-exponential and tri-exponential fitting curves with DW-signal plots. Representative fitting curves of bi-exponential and tri-exponential to all 12 b-value (0–2000) signal intensities were respectively presented in both sinonasal (a) and pharynx (b) SCC patients. Notably, the signal intensity in b-value of 2000 mm^2/s was better fitted in

the tri-exponential fitting than the bi-exponential fitting.

Fig. 3. Mono-exponential, SEM and DKI model fitting curves with DW-signal plots. Representative fitting curves of mono-exponential, SEM and DKI models to mainly targeted large b-value (b=0, 200, 400, 800, 1000 and 2000) signal data in both sinonasal (a) and pharynx (b) SCC patients. With these data, the mono-exponential model was not well fitted for the b-value of 2000 mm^2/s compared to the SEM and DKI model.

Figure1a

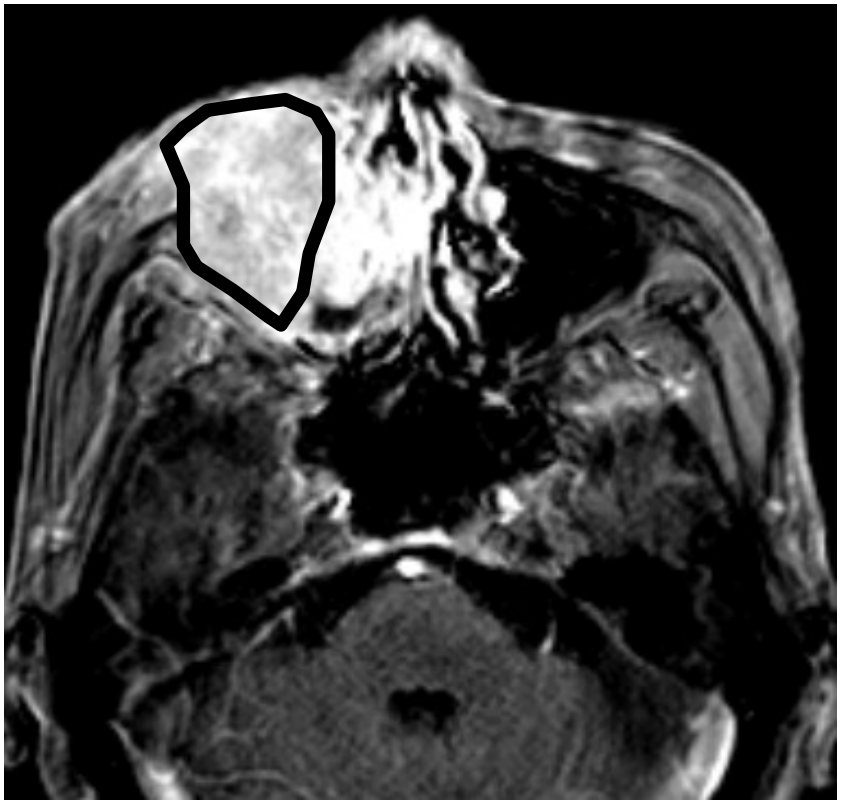

Figure1b

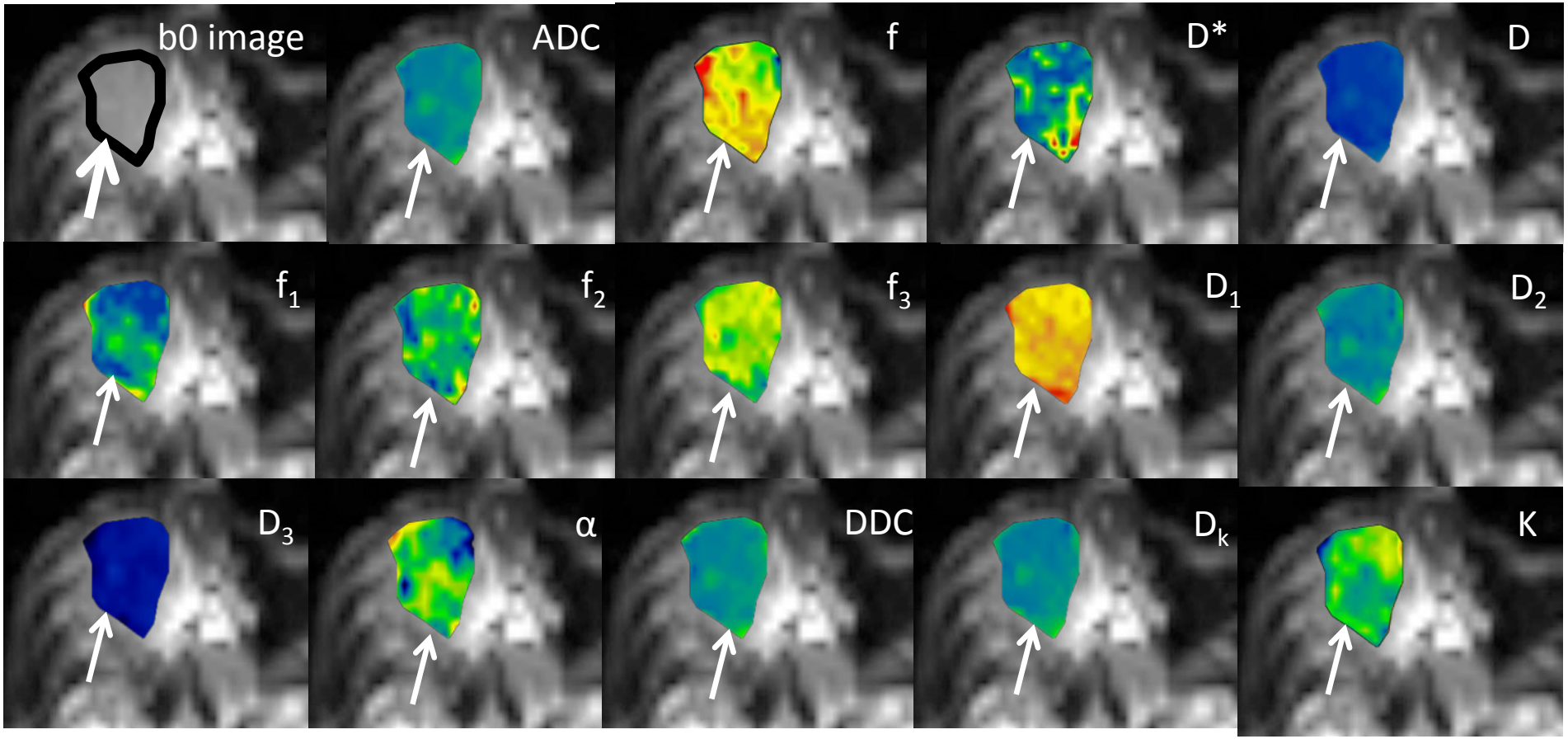

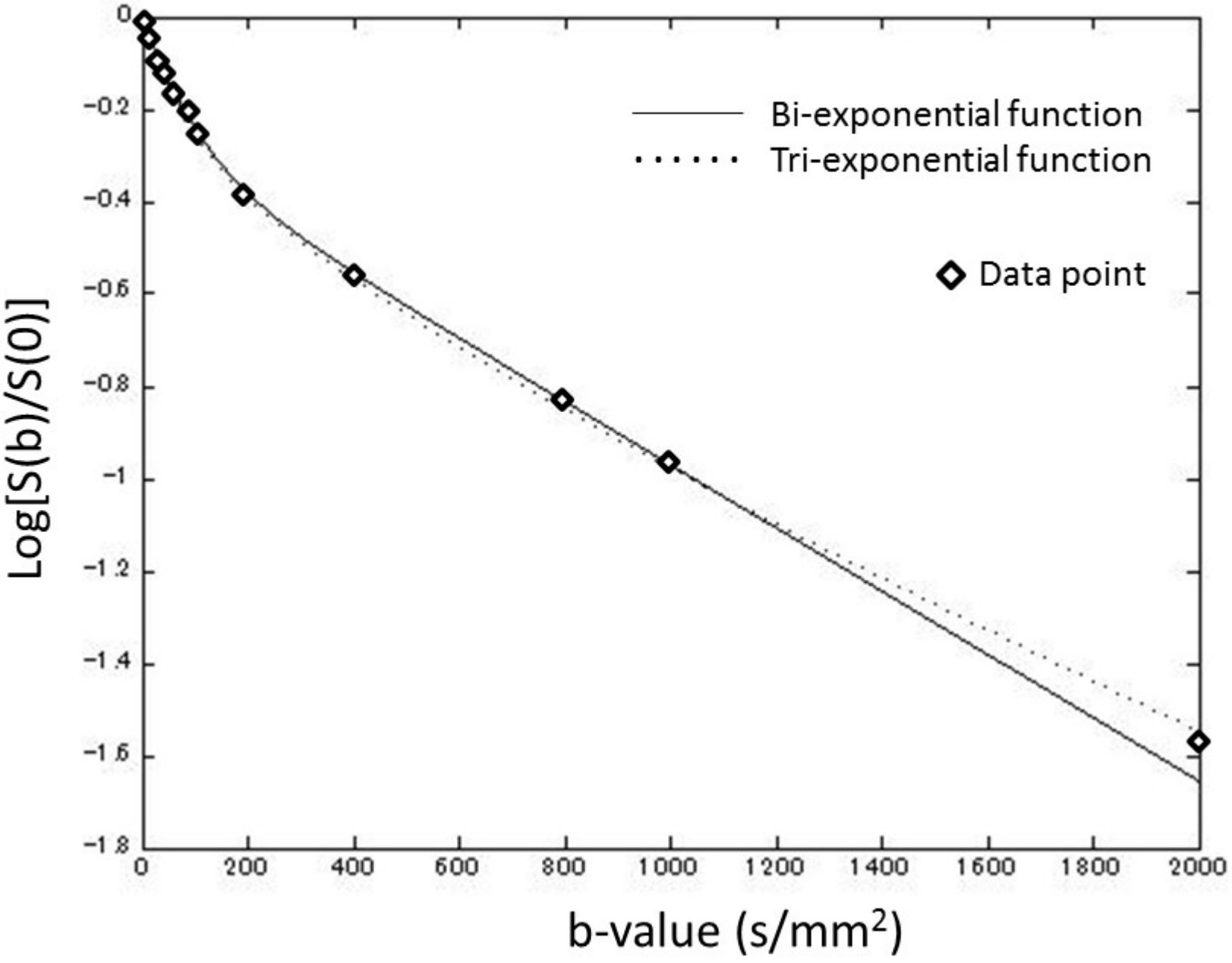
Bi-exponential function
Tri-exponential function
Data point
Log[S(b)/S(0)]
0
-0.2
-0.4
-0.6
-0.8
-1
-1.2
-1.4
-1.6
-1.8
0
200
400
600
800
1000
1200
1400
1600
1800
2000
b-value (s/mm²)

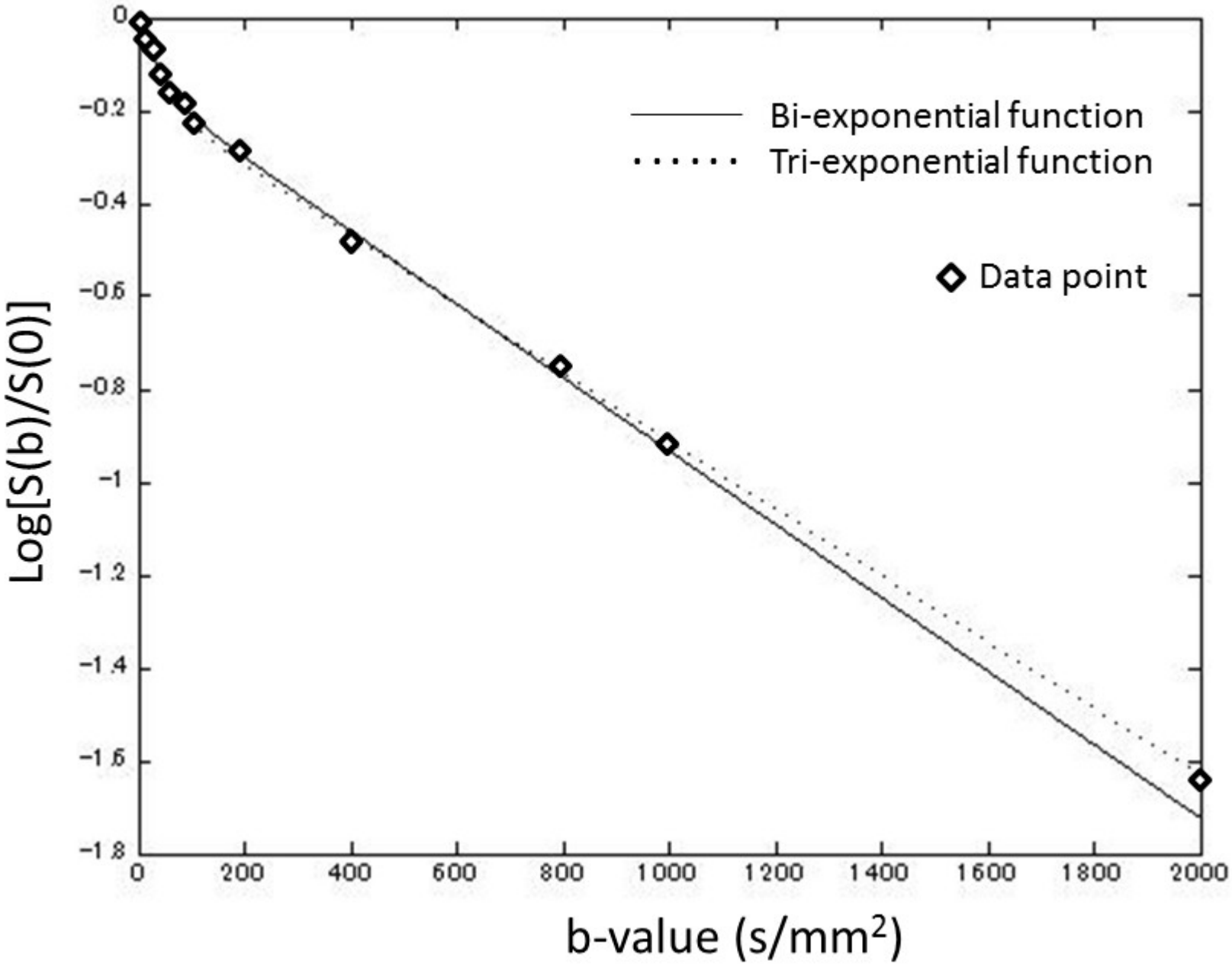
Bi-exponential function
Tri-exponential function
Data point
Log[S(b)/S(0)]
0
−0.2
−0.4
−0.6
−0.8
−1
−1.2
−1.4
−1.6
−1.8
0
200
400
600
800
1000
1200
1400
1600
1800
2000
b-value (s/mm²)

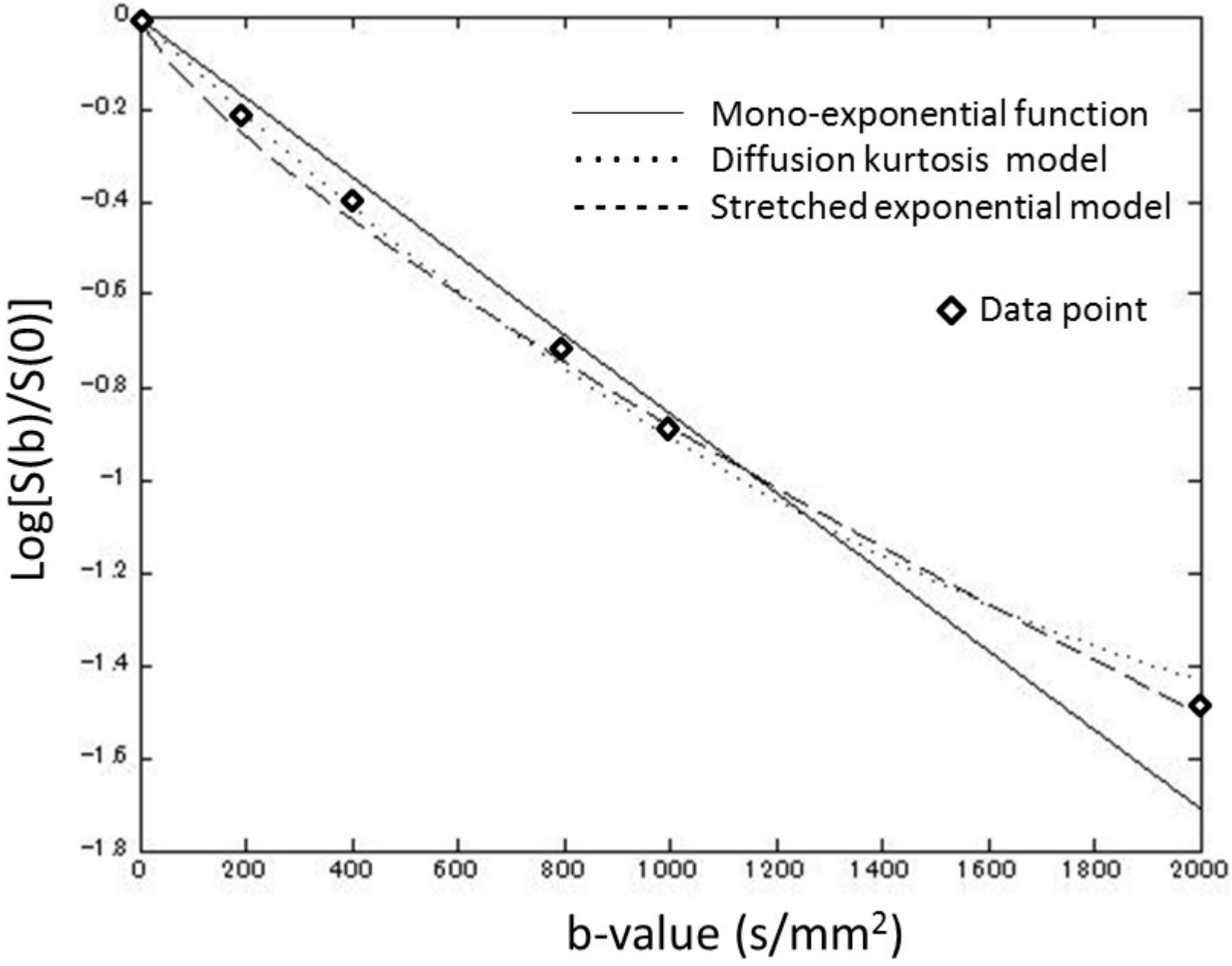
Mono-exponential function
Diffusion kurtosis model
Stretched exponential model
Data point
Log[S(b)/S(0)]
b-value (s/mm²)
0
-0.2
-0.4
-0.6
-0.8
-1
-1.2
-1.4
-1.6
-1.8
0
200
400
600
800
1000
1200
1400
1600
1800
2000

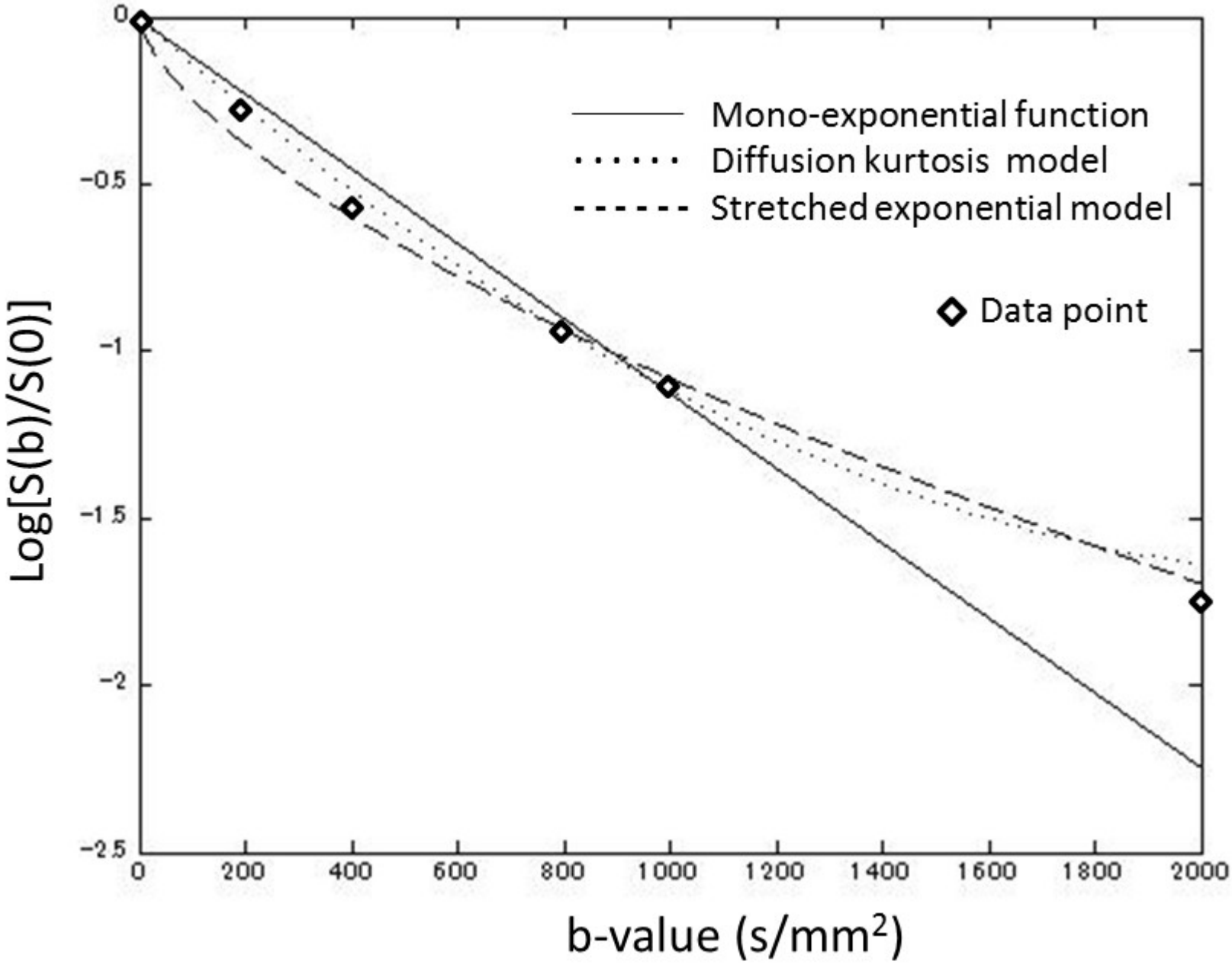
Mono-exponential function
Diffusion kurtosis model
Stretched exponential model
Data point
Log[S(b)/S(0)]
b-value (s/mm²)
0
-0.5
-1
-1.5
-2
-2.5
0
200
400
600
800
1000
1200
1400
1600
1800
2000